Brune, S., Babeyko, A. Y., Sobolev, S. V. (2009): Are tilt measurements useful in detecting tsunamigenic submarine landslides?. - Geochemistry Geophysics Geosystems (G3), 10, Q06002

DOI: 10.1029/2009GC002491

Are tilt measurements useful in detecting tsunamigenic submarine landslides?

Sascha Brune, Andrey Y. Babeyko, Stephan V. Sobolev

Helmholtz Centre Potsdam GFZ German Research Centre for Geosciences, Potsdam, Telegrafenberg, 14473 Potsdam, Germany

Abstract

Large submarine landslides can generate dangerous tsunamis. Due to their long period signal, detection of landslides by common seismological methods is difficult. Here, we suggest a method of detecting submarine landslides by using an array of land-based tiltmeters. The displacement of a large volume of sediments during landsliding produces a detectable elastic response of the lithosphere. We propose a technique to calculate this response and to invert for tsunami relevant parameters like slide location, volume and velocity. We exemplify our method by applying it to the Storegga slide west of Norway and other tsunamigenic landslide events. The parameter which can be most robustly estimated from tiltmeter array measurements is the product of slide volume and its velocity (slide tsunamigenic potential). This parameter also controls the amplitude of the generated tsunami wave. The inversion accuracy of this parameter and the estimated tsunami height near the coast depends on the noise level of tiltmeter measurements, distance of the tiltmeters from the slide, and slide tsunamigenic potential itself. The tsunamigenic potential of the most dangerous slides like Storegga can be estimated well by tiltmeters at the coast if the effective noise level does not exceed 50 nrad.

1 Introduction

Most tsunamis are generated by underwater earthquakes. Although submarine earthquakes in areas like the North Atlantic including the Norwegian Sea are small, the tsunami hazard can not be neglected. Some of the worlds largest submarine landslides have been identified in this region: the Storegga slide at the Norwegian continental slope (8200 years BP), the Hinlopen

slide north of Spitsbergen (probably pre-Holocene) and the Trænadjupet slide off Norway (4000 years BP) involving volumes of 2400 km³ (Bondevik et al. 2005), 1350 km³ (Vanneste et al. 2006) and 500 km³ (Laberg et al. 2002), respectively. The Storegga slide has been extensively studied (Bugge et al. 1987; Solheim et al. 2005), due to Norwegian oil-recovery interests in the head scarp area. Tsunami deposits of the Storegga event have been found in lake sediments of Norway, the Faroe Islands and on Scottish coasts. Run-up was reported as 10 m in Norway and even 20 m on the Shetland Islands (Bondevik et al. 2005). While these huge landslides occurred in the North Atlantic, there are numerous examples of tsunamigenic landslides in other parts of the world (Tinti et al. 2004; Okal et al. 2003; Yalçiner et al. 2003; Papadopoulos et al. 2007a;, McAdoo et al. 2000). Especially large events of the 20th century were the 1929 Grand Banks slide off Canada and the 1998 Aitape slump off Papua New Guinea. During these events sediment volumes of 200 km³ and 4 km³, respectively, failed (Fine et al. 2005; Synolakis et al. 2002). Also, as discussed by Berndt et al. (2009), a large slide west of Spitsbergen is possible.

While source parameters of tsunamigenic earthquakes can be determined in real-time with reasonable accuracy by classical seismological (e.g. Lomax et al. 2007) or novel GPS techniques (Blewitt et al. 2006; Sobolev et al. 2007), it is still very difficult to detect submarine landslides in the course of the event. Broadband seismic stations are not effective due to the comparatively small release of seismic energy and the long period signal. Although T waves of landslides can be identified in hydroacoustic and seismic records in the aftermath (Okal 2003), this technique is not yet applicable in real-time. GPS-buoys or ocean bottom pressure sensors are able to measure a tsunami during its passage (Kato et al. 2000; Gonzáles et al. 2005), but to quantify wave height and wave length, the arrival of the wave crest has to be waited for. If endangered coastal locations are close to the tsunami source, this loss of time may not be acceptable. An effective local tsunami early warning system requires the derivation of source parameters already during tsunami excitation. In the present paper, we propose a method to assess location, volume and velocity of submarine landslides using a tiltmeter array. We illustrate our method by applying it to the Storegga event and discuss its accuracy with respect to tsunami prediction.

2 Mathematical models

2.1 Tilt computation

Mass displacements produce an elastic deformation of the nearby lithosphere. Viscous effects are negligible, if the relevant time scale is much smaller than the Maxwell relaxation time which is in the order of 100 years for crust and upper mantle (based on Kennett and Engdahl (1991); Kennett et al. (1995)). Thus, with landslides lasting minutes to hours, elasticity clearly

dominates. We calculate tilt responses within the elastic half space approximation. The surface deformation due to a point load on an elastic half space (so-called Boussinesq problem) can be expressed in analytical terms. Considering the bulk landslide as an ensemble of point loads, the surface tilt at the surface point (x_1, x_2) is described by the expression (Farrell 1972, Boussinesq 1878):

$$\alpha_{1,2} = \frac{\partial u_3}{\partial x_{1,2}}$$

$$u_3 = -\left[\frac{1-\nu}{2\pi G} + \frac{f}{g^2}\right]\Phi$$

$$\Phi = \iint \frac{P(\varsigma_1, \varsigma_2)}{R(x_1, x_2, \varsigma_1, \varsigma_2)} d\varsigma_1 d\varsigma_2$$

$$R(x_1, x_2, \varsigma_1, \varsigma_2) = \left[(x_1 - \varsigma_1)^2 + (x_2 - \varsigma_2)^2\right]^{1/2}$$

We apply these formulas for the initial and the final sediment distribution. The measurable change in surface tilt due to the mass movement is calculated as the difference between final and initial tilt signal. The involved variables and parameter are: $\alpha_{1,2}$ - tilt in x- and y-direction (i.e. east and north, respectively), u_3 - vertical displacement (z-axis directed upwards), $x_{1,2}$ - point of observation, $\zeta_{1,2}$ - point of load, P - load distribution function, R - distance between $x_{1,2}$ and $\zeta_{1,2}$, f - gravitational constant ($6.67 \cdot 10^{-11}$ Nm^2kg^{-2}), g - standard gravity (9.81 ms^{-2}). As the deformation due to the dislocation involves large lithospheric portions, the involved parameters of the elastic half-space are evaluated at lithospheric depths (Kennett and Engdahl (1991); Kennett et al. (1995)): ν - Poisson's ratio (0.25), G - shear modulus ($7 \cdot 10^{10}$ Pa, corresponding to 100 km depth).

The measured surface inclination will be the result of two superposing effects, the removal of sediment and its deposit. Both are calculated with above formulas, whereas the removal contributes with a negative sign. The distance between the slide center of mass at the start and at the end of the movement, will be further on referred to as travel distance. This parameter has a crucial influence on the deformation. For small travel distances, like for slumps, removal and deposition areas overlap to a large extent. Hence, only a small resulting inclination of the free surface takes place. Assuming a constant sediment density, the load pressure distribution P is directly proportional to the slide's sediment distribution. In this paper we focus on landslide detection and not on detailed modeling of morphological features. So we use a simple non-

deformable slide shape parameterized by height, length, width, and orientation angle. Cross sections of the slide body consist of smooth polynomials, whose values and derivatives are zero at the edges. The full width at half maximum value corresponds exactly to a half of the overall length.

2.2 Storegga slide model

We exemplify this method by applying it to the Storegga event. In accordance with published bathymetry data and previous Storegga slide models, especially of Løvholt et al. (2005), the modeled slide body has a volume of 2400 km³ with a slide height of 220 m, length of 260 km and width of 180 km (Bryn et al. 2005; Bondevik et al. 2005). The center of mass moves from (4° 8' E, 63° 45' N) to (2° 3' E, 64° 45' N). Figure 1 depicts the movement in stereographically projected coordinates. The velocity profile is symmetrically composed out of sinusoidal segments. The sliding starts with an acceleration of 0.016 m/s², reaches a maximal velocity of 35 m/s and travels 150 km. These parameters have been calibrated against measured run-up heights of the Storegga slide (Løvholt et al. 2005).

2.3 Inversion technique

In section 2.1 we proposed a model that computes tilt signals for a given landslide event. To invert observed tilt signals into landslide parameters, we use this forward model together with the Matlab nonlinear minimization routine fminsearch (Matlab Version 7.1, copyright 1984–2005, The MathWorks, Inc. see also [Lagarias et al., 1998]) and minimize the root mean square of the difference between calculated and input tilt. To get a more stable inversion, we assume a rotationally symmetric slide shape in the forward model, parameterized by one variable only - the volume. The shape consists of smooth polynomials and is scaled self-similarly to match the given volume. The width to height ratio is 1500, so a 2400 km³ slide is 250 km wide and long, as well as 165 m high. Further inversion variables are initial slide position as well as the time-dependent displacement history of the slide.

In this study, the parameter setup was chosen as follows: We describe the displacement of the slide's center of mass at 6 different time points, corresponding to a time step of 20 minutes. Thus, the inversion calculates 13 output parameters: 6 locations of 2 coordinates and the landslide mass. Input parameters are the 5 non-zero tilt measurements (When the slide is still at the initial location, the tiltmeters do not yield a signal.) of each tiltmeter with 2 axes. Hence, 7 tiltmeter stations yield 70 input parameters. The system is over-determined. The final solution

results from the root mean square minimization of the difference between calculated and measured tilt signal.

2.4 Tsunami propagation model

We model tsunami propagation with the nonlinear Boussinesq code COULWAVE, using two vertical layers (Lynett and Liu 2002). The applicability condition (ratio of slide length to submergence depth must be larger than 7) is fulfilled due to a corresponding value of roughly 70. We project the sea bottom change, induced by the mass movement, directly towards the sea surface. So the propagating slide dynamically builds up the surface wave. The tsunami is calculated on a 900×750 grid with a spatial step size of 2500 m and a time step of 3 s. Resolution tests show that a grid refinement down to 1 km resulted in mareograms that were nearly identical to the 2.5 km time series. For reasons of efficiency, we use 2.5 km step size.

3 Landslide remote sensing via tiltmeters

3.1 Landslide detection

Figure 2 shows calculated tilt signals of our Storegga slide model. Virtual stations S1 to S5 are located in Norway, S6 on the Shetland Islands and S7 on the Faroes. All stations consist of two-axis tiltmeters which are oriented towards east and north for x- and y-direction, respectively. Station S1, which is nearest to the slide, exhibits maximum tilt values of approximately -2000 nrad for the x-component and 3000 nrad in y-direction. Regarding a present day tiltmeter accuracy of 1 nrad or less (d'Oreye and Zürn 2005; Ferreira et al. 2006; Gebauer et al. 2007), a huge landslide of the Storegga-scale will be clearly detectable.

3.2 Inversion for tsunami relevant parameters

As noted in section 2.3, we want to invert observed tilt signals into tsunami-relevant slide parameters such as initial position, volume and time-dependent displacement history. It is important to mention that modern tiltmeter precisions of several nanorad allow not only for landslide detection. Other events like tides, long period seismic wave passage or heavy rain are recorded as well. These processes superpose to landslide signals and thus degrade the quality of inversion. The latter will depend on the ability to exclude the secondary effects from tilt records. Advanced models can be used to correct for solid earth tides (McCarthy and Petit 2004). Furthermore, characteristic times of landslides movement range between several minutes for small events up to about one hour in case of huge slides. Filtering for the corresponding frequency range will exclude noise signals of different time periods.

Despite these correction routines, a certain amount of "effective" noise will remain within the data. We investigate how this residual perturbance affects the inversion by adding white noise to the synthetic tilt data of our model before inverting. We examine three noise amplitudes: 20, 50 and 100 nrad, and invert 20 different data samples for each noise level. Inversion results together with the original model are shown in Figure 3B. We find good inversion results for the noise levels of 20 and 50 nrad, and rather poor results for 100 nrad.

We assume the product of maximum velocity and volume as a measure for the slide tsunamigenic potential (Løvholt et al. 2005). As maximum velocities of slides are very difficult to determine, this relation has not been proven yet. Nevertheless, we consider it here as a reasonable assumption. As depicted in Figure 3C, this parameter deviates not more than 10 % from the original value in cases of 20 and 50 nrad. A noise amplitude of 100 nrad again does not yield satisfying correspondence. Interestingly, volume and maximum velocity are under- and overestimated, respectively. This discrepancy results from different geometries of the original scenario (elongated source) and the rotationally symmetrical forward model of the inversion. Tsunami predictions based on the inversion results are discussed in section 4.

The number of implemented tiltmeters and their distribution affects the quality of the inversion. In principle, the inversion can be done if only two tilt stations exist (see section 2.3), however, due to noise, the inversion quality increases significantly if more stations are used. The quality saturates in the Storegga case if about 7-9 tilt stations are used. We conducted a series of experiments involving different number and position of tiltmeters. We found best results, if the stations cover a large coastal area around the slide. For instance, the positioning of two stations on the Shettland and Faroe Islands instead in Norway increases the inversion quality.

Large submarine slide bodies tend to disintegrate during the landslide event (Haflidason et al. 2005). Effectively, the disintegration leads to a dynamic decrease of slide height and an increase of slide length (the slide dimension parallel to the slope). To test the possible effect of the slide disintegration, we model the slide deformation during the movement by enlarging the length of our Storegga slide body while simultaneously adjusting its thickness to conserve the volume. We describe the dynamic slide deformation by the following expression:

$$\boldsymbol{l}(\boldsymbol{t}) = \boldsymbol{l}(0) + 2 \cdot \boldsymbol{Deform} \cdot \boldsymbol{s}(\boldsymbol{t})$$

where *l(t)* is time-dependent slide length, *h(t)* slide width, *s(t)* travel distance and *Deform* is a non-dimensional parameter varying continuously between 0 and 1. *Deform* = 0 conserves the

slide length, while *Deform* = 1 produces maximum deformation. For values larger than 1, the upper slide end would propagate up-slope which is unphysical. In case of the Storegga slide with 150 km travel distance, maximal deformation (*Deform* = 1) corresponds to a slide length increase from 260 km to 560 km while the height decreases from 220 m to 100 m.

Figure 4 shows the influence of the slide deformation on our inversion results. We compare inversion results for three equal-volume but different shaped models (*Deform* = 0, 0.5 and 1). Generally, inversion results demonstrate low sensitivity to the slide deformation. Inverted trajectories (Figure 4B) as well as maximum velocities and volumes (Figure 4C) differ only slightly. The influence on the tsunamigenic potential is also rather small: the product of volume and maximum velocity decreases by 10 % for *Deform*=0.5 and ~20 % for *Deform*=1.

Finally, we address the question of reliability of our inversion for different slide geometries. Since the exact shape of a landslide is not known during the event, we invert tilt observations using a rotationally symmetric slide body as described in section 2.3. Moreover, this constraint gives us more stable inversion results. To check reliability and robustness of this assumption, we apply our inversion procedure to slide bodies with aspect ratios of 0.5, 0.7 and 1 while keeping the volume and height constant (Figure 5). Large slides like Storegga (aspect ratio 0.7, see section 2.2) tend to be elongated in direction parallel to the slide movement, so we focused on this direction of elongation. As expected, our inversion yields best results for the forward model with aspect ratio 1, which corresponds to the rotationally symmetric slide body of the inversion procedure. The discrepancies of location, volume and maximal velocity grow up to 50 % for strongly elongated slides. However, the tsunamigenic potential of the event, which is the product of volume and maximum velocity, was estimated within 20 % of the original value. Thus, we can conclude that the tsunamigenic potential of a landslide of any shape can be predicted rather reliable and robustly even if the original geometry strongly differs from rotationally symmetrical.

4 Tsunami prediction

The previous section shows that despite some under- and overestimation of particular slide parameters, the inversion procedure, nevertheless, yields good results for the tsunamigenic potential of a landslide. To further illustrate this idea, we directly oppose resulting tsunami impact from the original Storegga model to that of inverted models with 20, 50 and 100 nrad noise (compare Figure 3). The maximum wave height of the tsunami for the original scenario is shown in Figure 6A. Near-shore maximum wave heights reach up to 7 m in Norway. Arrival

times are 1.5 to 4 h at the Norwegian coast, about 1 h at the Shetland and Faroe islands, 2 h for Iceland and 3 to 5 hours for the Scottish mainland.

To check inversions against the original model, we perform tsunami calculations based on the inverted slide parameters of each considered noise level (20, 50 and 100 nrad). Therefore, five representative scenarios (including end members) where chosen among the 20 inversion results of each noise level (see section 3.2). Outliers for noise of 100 nrad which show unreasonably high velocities of 100 m/s were excluded from the tsunami simulations. Mareograms of the considered scenarios are compared to the original scenario in Figure 6B. Arrival times and wave forms correspond very well, while the amplitude increases with noise from about 10 % for 20 and 50 nrad, to 40 % for 100 nrad. The corresponding ranges of maximum wave heights for every noise level are displayed as gray bars in Figure 6C. The maximum wave height of the original scenario, for comparison, is shown in red. Again, we find satisfying correspondence between original scenario and 20 nrad as well as 50 nrad noise data. The maximum wave heights at the gauges should not be mistaken for run-up values, whose computation necessitates detailed bathymetry information, especially in fjords, and additional numerical treatment.

5 Estimating the applicability scope

We have demonstrated above that our suggested method may work very well for the Storegga landslide. However, the Storegga event was exceptionally large. In this section, we study the applicability of our method to mass movements with smaller slide volumes. Therefore, we first define two distinct qualities: (a) We call an event detectable if the slope failure generates a tilt signal that is larger than the detectability threshold T_d. (b) We assume the existence of an invertibility threshold T_i, that has to be exceeded by a tilt amplitude, in order to ensure the invertibility for correct location and tsunamigenic potential. In principle, both T_d and T_i depend on the concrete setting of each scenario. For simplification, however, we estimate approximate values: Detectability is guaranteed, if signal to noise ratios are large. Assuming an effective noise level of 20 nrad, signal to noise ratios of at least 10 are reached if tilt amplitudes exceed 200 nrad. We will use this value to approximate T_d.

To determine the invertibility threshold T_i, the inversion routine has to be applied to different tilt amplitudes. We therefore consider a series of scenarios that resemble the Storegga event, but involve different slide volumes. We modify the slide height, while the slide length, width, trajectory, and tiltmeter positions remain identical to the original Storegga scenario. 14 scenarios are considered, with volumes ranging between 165 km³ and 2400 km³. For every setup, we

perform 100 inversions, each time with new white noise added to the signals. We consider an inversion successful, if the inverted tsunamigenic potential lies within ±20 % range of the original value. The percentage of successful inversions for each scenario is shown in Figure 7A. For small tilts, inversions are not reliable, though with growing size, the number of successful inversions increases rapidly and finally starts to saturate, if maximum tilt signals exceed ~1000 nrad. Generalizing this result, we will use that value from now on as invertibility threshold T_i.

For each scenario, Figure 7B depicts the maximum near shore tsunami heights of the virtual gauge at Sula (the gauge closest to the slide, see Figure 6). As expected, wave heights grow linearly with the tsunamigenic potential, which in this case depends on the volume only. T_i is exceeded for scenarios that induce more than 2.5 m tsunami amplitude. This means that in the Storegga case, good tsunami predictions based on tilt inversion are possible for all wave heights larger than 2.5 m. Although events with smaller tsunami amplitudes cannot be inverted, they can still be detected. For Storegga-like scenarios, the above discussed detectability threshold of 200 nrad implies the detection of events that induce more than 0.7 m wave amplitude.

Using these values for T_d and T_i, we estimate the scope of our landslide detection tool by applying it to many hypothetical events. For each event we address the question, if the detectability threshold or even the invertibility threshold is exceeded. The ensemble of events is characterized by the fundamental parameters slide volume, travel distance, and distance between slide and tiltmeter. We calculate the tilt amplitudes of numerous scenarios that cover a large range with respect to slide volume (0.1-3000 km³) and travel distance (1-1000 km). We use a simplified geometry, where the slide moves perpendicular to a straight coastline and one tiltmeter is positioned at the nearest coastal point. The slide shape is rotationally symmetrical and self-similar, analog to that described in section 2.3. Since the value of the shear modulus should be evaluated at a depth corresponding to the distance between slide and tiltmeter, we linearly approximate the shear modulus as a function of depth in a way that it is $4 \cdot 10^{10}$ Pa and $7 \cdot 10^{10}$ Pa in a depth of 10 km and 100 km, respectively. These values are based on Kennett and Engdahl (1991) as well as Kennett et al. (1995).

For each scenario with given slide volume and travel distance, there exists a distance between tiltmeter and slide start, so that the tilt signal drops below the detectability or invertibility threshold. These distances are depicted as colored lines in Figure 8A and 8B, respectively. The distance-volume dependency is approximately linear in the double logarithmic plot, thus distance is proportional to volume to the constant power. As discussed above, the travel distance has

crucial influence on the surface deformation. That is why lines representing long travel distances, e.g. translational slides, are located above lines of small dislocation which represent slumps. For long travel distances and small volumes, the final deformation does not depend on the dislocation of the slide anymore. Thus curves of big travel distance converge at small volumes. Scenarios that do not produce tilt signals which exceed the required threshold T_d or T_i are not shown. This is the case in Figure 8B, for travel distances that are smaller than 10 km and for small volumes of the order of 1 km³ and below.

We superimpose parameters of past and possible tsunamigenic landslide events onto Figure 8A. Each event is represented by a triplet of data (volume, travel distances and distance to coast), shown in Table 1. If the data point lies above the curve of corresponding travel distance (shown as circle) the necessary distance for detection is not reached and the slide could not have been detected. This is the case for the Aitape event of 1998, for the Grand Banks slide in 1929, as well as for the Sumba slide. If the data point is situated below the corresponding curve (designated as large star), the detection would have been possible, as for the Palos Verdes avalanche, the Oshima-Oshima volcanic landslide of 1741, the Hawaiian Alika debris avalanche, the Hinlopen and Storegga slide. The possible Spitsbergen event would be detectable as well. The Nice landslide of 1979, the Unimak event of 1946, as well as the Albemarle-Currituck slide off the U.S. mid-Atlantic coast are situated very close to the detection boundary (shown as small stars).

Applying the same procedure in Figure 8B, we see that the inversion of an event requires a smaller slide-tiltmeter distance than its detection. Inversion is clearly possible for the large tsunamigenic slides of the North Atlantic and Hawaii. Although the Unimak and the Albemarle-Currituck events are detectable, they are possibly not invertible. The Nice slide and the Palos Verdes avalanche, due to their small travel distance of several kilometers, did not produce tilt signals larger than T_i.

In this publication, we focus on the remote detection of large submarine landslides. However, smaller landslides can be tsunamigenic as well: Skagway 1994 (Kulikov et al. 1996), Fatu Hiva, 1999 (Hébert et al. 2002), Stromboli, 2002 (Maramai et al. 2005), Corinth Gulf, 1963 (Papadopoulos et al. 2007b) or Amorgos Basin (Perissoratis and Papadopoulos 1999). In principle, our technique can be applied for these cases as well, although the distance between slide center and tiltmeter has to be quite small (in the order of 1 km). Our technique is not applicable if the required distance is smaller than the half of a slide length, as the tiltmeters have to be located outside the failure zone.

6 Conclusions

In the present study, we propose a method of using tiltmeters to detect submarine landslides. In principle, this is possible during the event allowing for fast detection of a possible tsunami. Using a numerical modeling technique, we apply our method to the Storegga event, where resulting tilt amplitudes are in the order of several 1000 nrad at the nearest stations. As present day tiltmeter accuracy amounts to several nrad, a landslide of this size would be clearly detectable.

This publication is as far as we know one of the first to describe the detection of submarine landslides and the inversion based on tiltmeter measurements. Although our theoretical simulations yield promising results, thorough experimental verifications will have to be conducted before the method is implementable in future tsunami warning systems.

Tilt measurements can be inverted for tsunami relevant parameters. Inversions for the slide tsunamigenic potential (product of volume and maximum velocity) are in good agreement with original data if tiltmeter noise level stays below 50 nrad. Consequently, inverted landslide parameters can be used to estimate near-coast tsunami wave heights. Theoretical tsunami predictions based on the inverted scenarios correspond well to the original tsunami with respect to arrival time and maximum wave height. Our inversion technique yields satisfying results for deforming slides as well as for elongated or circular slide geometries. Thus, the tsunami hazard associated with a submarine landslide can be assessed with good accuracy, even if the explicit original geometry is not known.

We evaluate the conditions, under which the detection of submarine mass movements by means of tiltmeters is possible. Past events like the Hinlopen slide, the Storegga event and the Alika slide could have been detected and inverted. In general, longer travel distances leading to larger deformations are favored by our method.

Acknowledgements

This is publication 26 of the GITEWS project (German Indonesian Tsunami Early Warning System). The project is carried out through a large group of scientists and engineers from GeoForschungsZentrum Potsdam (GFZ) and its partners from DLR, AWI, GKSS, IFM-

GEOMAR, UNU, BGR, GTZ, as well as from Indonesian and other international partners. Funding is provided by the German Federal Ministry for Education and Research (BMBF), grant 03TSU01.

References

Assier-Rzadkiewicz, S., P. Heinrich, P. C. Sabatier, B. Savoye and J. F. Bourillet (2000), Numerical Modelling of a Landslide-generated Tsunami: The 1979 Nice Event, *Pure Appl. Geophys.*, 157, 1707–1727.

Berndt, C., S. Brune, E. Nisbet, J. Zschau, S. V. Sobolev (2009), Tsunami modeling of a submarine landslide in the Fram Strait. *Geochem. Geophys. Geosys.*, doi:10.1029/2008GC002292.

Blewitt, G., C. Kreemer, W. C. Hammond, H. P. Plag, S. Stein, E. Okal (2006), Rapid determination of earthquake magnitude using GPS for tsunami warning systems, *Geophys. Res. Lett.*, 33, L11309, doi:10.1029/2006GL026145.

Bondevik, S., F. Løvholt, C. Harbitz, J. Mangerud, A. Dawson, J.I. Svendsen (2005), The Storegga Slide tsunami—comparing field observations with numerical simulations, *Mar. Pet. Geol.*, 22,195–208.

Boussinesq, J. V. (1878), Équilibre d'élasticité d'un sol isotrope sans pesanteur, supportant différents poids. *C. R. Math. Acad. Sci. Paris,* 86 , 86, 1260-1263.

Bryn, P., K. Berga, C.F. Forsberg, A. Solheim, T. J. Kvalstad (2005), Explaining the Storegga Slide, *Mar. Pet. Geol.*, 22, 11–19.

Bugge, T., S. Befring, R. H. Belderson, T. Eidvin, E. Jansen, N. H. Kenyon, H. Hoitedahi, and H. P. Sejrup (1987), A Giant Three-Stage Submarine Slide Off Norway, *Geo-Mar. Lett.*, 7, I91-198.

d'Oreye, N. F., W. Zürn (2005), Very high resolution long-baseline water-tube tiltmeter to record small signals from Earth free oscillations up to secular tilts, *Rev. Sci. Instrum.*, 76, 024501.

Driscoll, N. W., J. K. Weissel, J. A. Goff (2000), Potential for large-scale submarine slope failure and tsunami generation along the U.S. mid-Atlantic coast, *Geology,* 28(5), 407–410.

Farrell, W. E. (1972) Deformation of the earth by surface loads. *Rev Geophys Space Phys.* 10(3):762-797.

Ferreira, A. M. G., N. F. d'Oreye, J. H. Woodhouse, W. Zürn (2006), Comparison of fluid tiltmeter data with long-period seismograms: Surface waves and Earth's free oscillations. *J Geophys Res.,* VOL. 111, B11307, doi:10.1029/2006JB004311.

Fine, I. V., A. B. Rabinovich, B. D. Bornhold, R. E. Thomson, E. A. Kulikov (2005), The Grand Banks landslide-generated tsunami of November 18, 1929: preliminary analysis and numerical modeling, *Mar. Geol.*, 215, 45-57.

Gebauer, A., T. Jahr, G. Jentzsch (2007), Recording and interpretation/analysis of tilt signals with five ASKANIA borehole tiltmeters at the KTB, *Rev. Sci. Instrum.*, 78, 054501.

Gonzáles, F. I., E. N. Bernard, C. Meinig, M. C. Eble, H.O. Mofjeld, S. STALIN (2005), The NTHMP Tsunameter Network, *Nat. Hazards*, 35: 25–39.

Haflidason, H., R. Lien, H. P. Sejrup, C. F. Forsberg, P. Bryn (2005), The dating and morphometry of the Storegga Slide, *Mar. Pet. Geol.,* 22, 123–136.

Hébert, H., A. Piatanesi, P. Heinrich, and F. Schindelé (2002), Numerical modeling of the September 13, 1999 landslide and tsunami on Fatu Hiva Island (French Polynesia), *Geophys. Res. Lett.*, 29(10), 1484.

Kato, T., Y. Terada, M. Kinoshita, H. Kakimoto, H. Isshiki, M. Matsuishi,
A. Yokoyama, T. Tanno (2000), Real-time observation of tsunami by RTK-GPS
Earth Planets Space, 52, 841–845.

Kennett, B. L. N., E. R. Engdahl (1991), Travel times for global earthquake location and phase identification. *Geophys J Int.* 105:429-465.

Kennett B. L. N., E. R. Engdahl, R. Buland (1995), Constraints in seismic velocity in the earth from travel times. *Geophys J Int.* 122:108-124.

Kulikov, E. A., A. B. Rabinovich, R. E. Thomson, B. D. Bornhold (1996), The landslide tsunami of November 3, 1994, Skagway Harbor, Alaska. *J Geophys Res.* 101(C3):6609-6615.

Laberg, J. S., T. O. Vorren, J. Mienert, P. Bryn, R. Lien (2002), The Trænadjupet Slide: a large slope failure affecting the continental margin of Norway 4,000 years ago, *Geo-Mar. Lett.*, 22, 19–24.

Lagarias, J. C., J. A. Reeds, M. H. Wright, and P. E. Wright (1998), Convergence Properties of the Nelder-Mead Simplex Method in Low Dimensions, *SIAM J. Optim.*, 9(1), 112-147.

Locat, J., H. J. Lee, P. Locat, J. Imran (2004), Numerical analysis of the mobility of the Palos Verdes debris avalanche, California, and its implication for the generation of tsunamis, *Mar. Geol.,* 203, 269-280.

Lomax, A., A. Michelini and A. Piatanesi (2007), An energy-duration procedure for rapid determination of earthquake magnitude and tsunamigenic potential, *Geophys. J. Int*., 170, 1195-1209.

Løvholt, F., C. B. Harbitz, K. B. Haugen (2005), A parametric study of tsunamis generated by submarine slides in the Ormen Lange/Storegga area off western Norway, *Mar. Pet. Geol.*, 22, 219–231.

Lynett, P., P. L. F. Liu, (2002), A numerical study of submarine-landslide-generated waves and run-up, *Proc. Roy. Soc. A*, 458, 2885

Maramai, A., L. Graziani, G. Alessio, P. Burrato, L. Colini, L. Cucci, R. Nappi, A. Nardi, G. Vilardo (2005), Near- and far-field survey report of the 30 December 2002 Stromboli (Southern Italy) tsunami, *Mar. Geol.*, 215, 93-106.

Matlab Version 7.1, Copyright 1984-2005, The MathWorks, Inc.

McAdoo, B. G., L. F. Pratson, D.L. Orange (2000), Submarine landslide geomorphology, US continental slope. *Mar. Geol.*, 169 (2000) 103–136.

McCarthy, D., and Petit G. (eds). (2004). IERS Conventions (2003). IERS Technical Note No 32, *Verlag des Bundesamts fur Kartographie und Geodasie*, Frankfurt am Main, 127pp.

McMurtry, G. M., P. Watts, G. J. Fryer, J. R. Smith, F. Imamura (2004), Giant landslides, mega-tsunamis, and paleo-sea level in the Hawaiian Islands, *Mar. Geol.*, 203, 219-233.

Normark, W. R., M. McGann, R. Sliter (2004), Age of Palos Verdes submarine debris avalanche, southern California, *Mar. Geol.*, 203, 247-259.

Okal, E. A., G. Plafker, C. E. Synolakis, J. C. Borrero (2003), Near-Field Survey of the 1946 Aleutian Tsunami on Unimak and Sanak Islands, *Bull. Seism. Soc. Am.*, 93(3), 1226–1234.

Okal, E. A. (2003), T Waves from the 1998 Papua New Guinea Earthquake and its Aftershocks: Timing the Tsunamigenic Slump, *Pure Appl. Geophys.*, 160, 1843–1863.

Papadopoulos, G. A., E. Daskalaki, A. Fokaefs (2007a), Tsunamis generated by coastal and submarine landslides in the Mediterranean Sea, in: *Submarine Mass Movements and Their Consequences*, *Adv. Nat. Tech. Hazards Res.,* vol 27, edited by V. Lykousis, D. Sakellariou, J. Locat, Springer, Dordrecht, pp 327-336.

Papadopoulos, G. A., L. I. Lobkovsky, R. K. Mazova, I. A. Garagash, V. Karastathis, L. Y. Kataeva, V. G. Kaz'min (2007b), Numerical Modeling of Sediment Mass Sliding and Tsunami Generation: The Case of February 7, 1963, in Corinth Gulf, Greece, *Mar. Geodesy*, 30(4), 315-331.

Perissoratis, C., G. Papadopoulos (1999), Sediment instability and slumping in the southern Aegean Sea and the case history of the 1956 tsunami, *Mar. Geol.*, 161, 287–305.

Satake K., Y. Kato (2001), The 1741 Oshima-Oshima Eruption: Extent and Volume of Submarine Debris Avalanche, *Geophys. Res. Lett.*, 28(3), 427-430.

Sobolev, S. V., A. Y. Babeyko, R. Wang, A. Hoechner, R. Galas, M. Rothacher, D. V. Sein, J. Schröter, J. Lauterjung, and C. Subarya (2007), Tsunami early warning using GPS-Shield arrays, *J. Geophys. Res.*, 112, B08415, doi:10.1029/2006JB004640.

Solheim, A., P. Bryn, H. P. Sejrup, J. Mienert, K. Berg (2005), Ormen Lange - an integrated study for the safe development of a deep-water gas field within the Storegga Slide Complex, NE Atlantic continental margin; executive summary, *Mar. Pet. Geol.*, 22, 1–9.

Synolakis, C. E., J.-P. Bardet, J. C. Borrero, H. L. Davies, E. A. Okal, E. A. Silver, S. Sweet and D. R. Tappin (2002), The slump origin of the 1998 Papua New Guinea Tsunami. *Proc. R. Soc. Lond.* A 458, 763–789.

Tinti S., A. Maramai , L. Graziani (2004), The new catalogue of Italian tsunamis Source: *Nat. Hazards*, 33(3), 439-465.

Vanneste, M., J. Mienert, S. Bünz (2006), The Hinlopen Slide: A giant, submarine slope failure on the northern Svalbard margin, Arctic Ocean, *Earth Planet. Sci. Lett.,* 245, 373–388.

Watts, P., S. T. Grilli, J. T. Kirby, G. J. Fryer, and D. R. Tappin (2003), Landslide tsunami case studies using a Boussinesq model and a fully nonlinear tsunami generation model, *Nat. Hazards Earth Sys. Sci.*, 3, 391–402.

Winkelmann, D., W. Jokat, F. Niessen, R. Stein, and A. Winkler (2006), Age and extent of the Yermak Slide north of Spitsbergen, Arctic Ocean, *Geochem. Geophys. Geosys.*, 7(6), doi:10.1029/2005GC001130.

Yalçiner A. C, E. Pelinovsky, E. Okal, C. E. Synolakis (2003), Submarine Landslides and Tsunamis. NATO Sci Ser. Ser. IV, vol. 21, 327 pp. Kluwer Acad., Norwell, Mass.

Table

Event (year)	Volume (km^3)	Travel distance (km)	Distance to coast (km)	References
Aitape, Papua New Guinea (1998)	4	0.84	30	(Synolakis et al. 2002)
Nice, France (1979)	0.15	5	5	(Assier-Rzadkiewicz et al. 2000)
Unimak, Alaska, USA (1946)	120	179	80	(Watts et al. 2003; Okal et al. 2003)
Grand Banks, Canada (1929)	200	200	280	(Fine et al. 2005)
Oshima-Oshima, Japan (1741)	2.5	10	5	(Satake and Kato, 2001)
Hinlopen, Norway (4000 BP)	1350	100	100	(Vanneste et al. 2006; Winkelmann et al. 2006)
Palos Verdes, Cali-fornia, USA (7500 BP)	0.73	5	6	(Locat et al. 2004; Normark et al. 2004)
Storegga, Norway (8200 BP)	2400	150	100	(Haflidason et al. 2005)
Alika, Hawaii, USA (100 000 BP)	400	100	100	(McMurtry et al. 2004)
Sumba, Indonesia (age unknown)	95	10	135	(Brune et al. in prep.)
Albemarle-Currituck, Virginia, USA (age unknown)	150	100	100	(Driscoll et al. 2000)
Spitsbergen, Norway (possible)	1000	60	80	(Berndt et al. 2009)

Table 1 Slide parameters used in Figure 8. The minimal distance to position a tiltmeter near a slide was associated with the distance to the coast. The Alika slide represents the first Alika event, however, the second Alika avalanche exhibited similar features (McMurtry et al. 2004).

As the Oshima-Oshima volcanic avalanche was partly subaerial, the distance to the coast is effectively zero. We use a distance between virtual tiltmeter and slide center of 5 km, assuming that the tiltmeter is positioned on the distant side of the island.

Figures

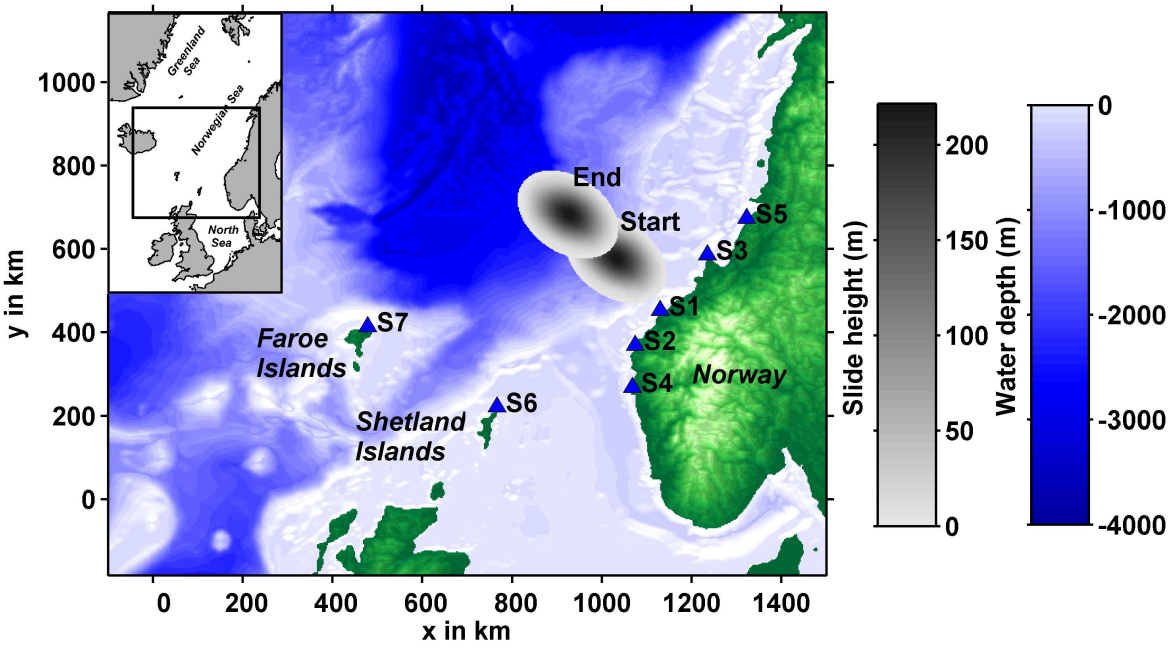

Figure 1 Storegga slide model. Sediment distributions at the beginning and the end of the event are shown in gray. Blue triangles depict locations of virtual tiltmeter stations S1 to S7.

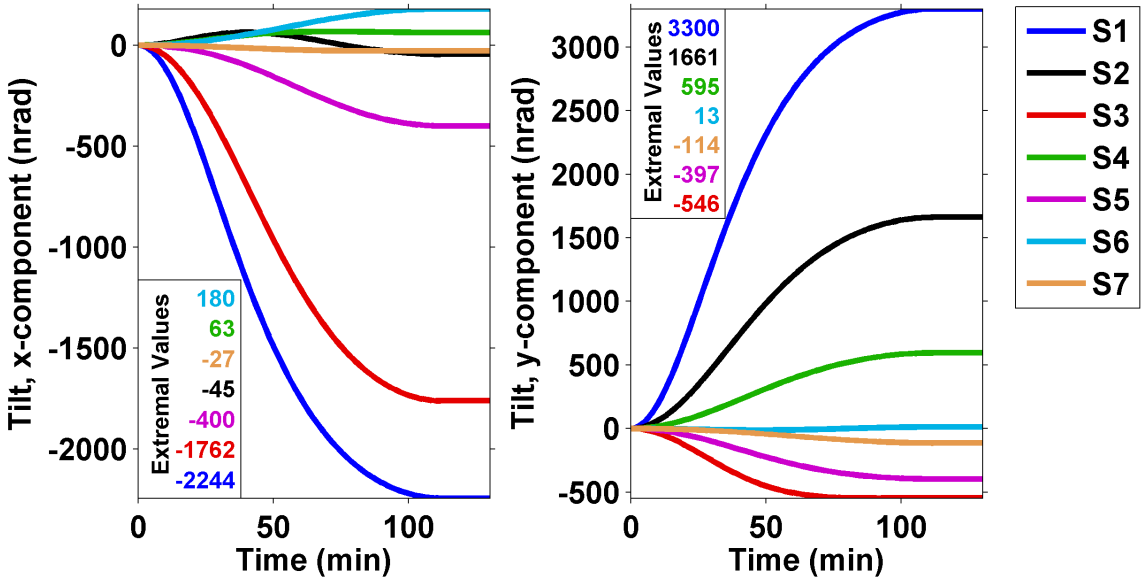

Figure 2 Computed tilt signals in x- and y-direction of the Storegga event. Positions of tilt stations S1 to S7 are mapped in Figure 1.

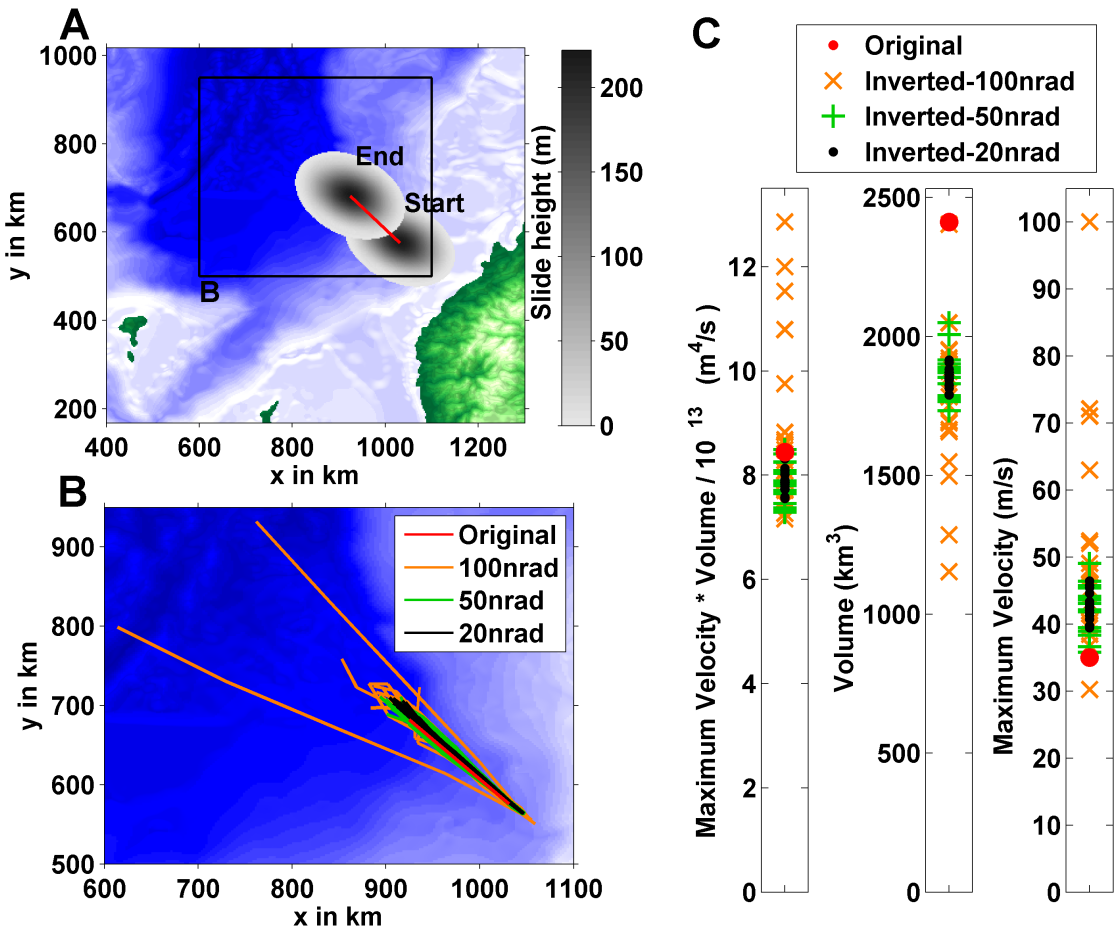

Figure 3 Storegga slide inversion: Influence of noise level **(A)** Storegga slide model setup. The red line indicates the center of mass trajectory. **(B)** Original (see A) and inverted center of mass trajectories for noise amplitudes of 20, 50 and 100 nrad. **(C)** Inverted and original values for the tsunami-relevant product of volume and maximum velocity and both of them alone.

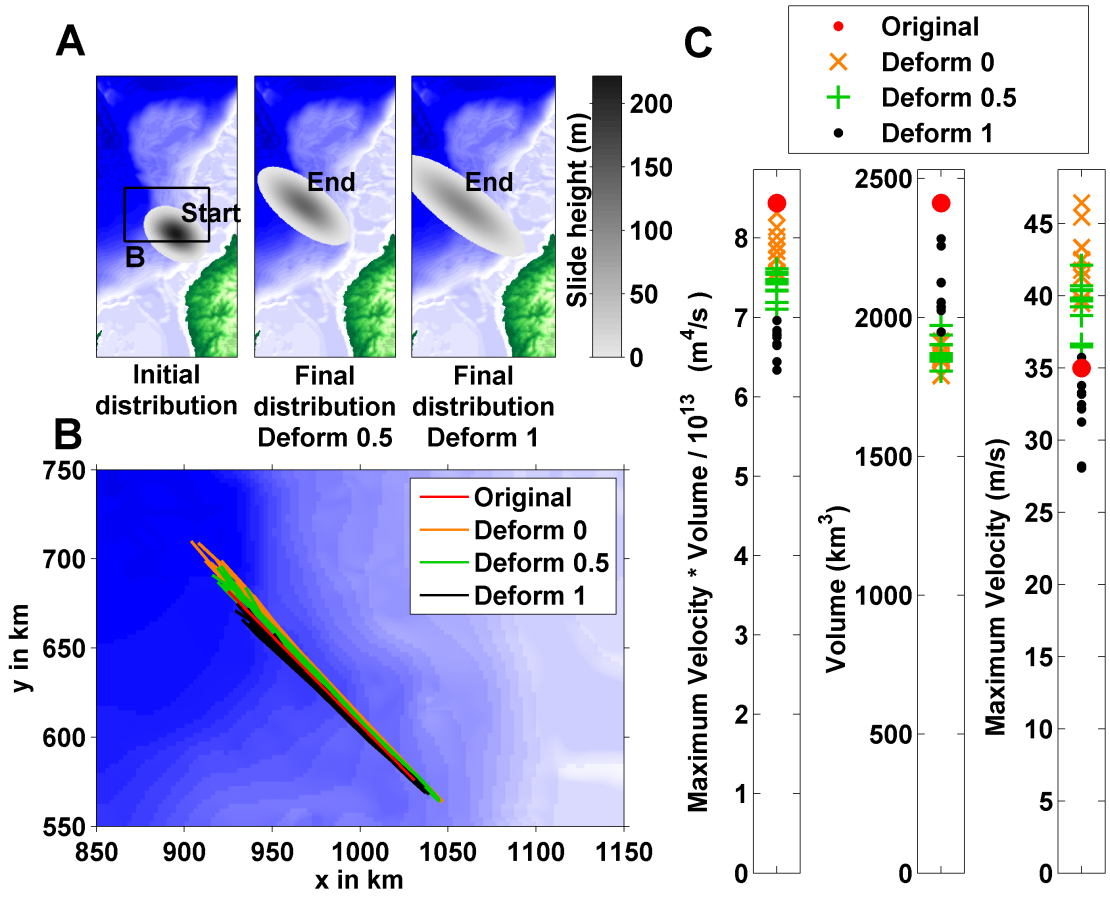

Figure 4 Influence of slide deformation on inversion results (Noise level: 20 nrad). **(A)** Slide models with identical volumes, but different deformation factor (see section 3.2): Deform= 0, 0.5, 1. Thereby Deform=0 corresponds to the original Storegga discussed before. **(B)** Inverted and original center of mass trajectories. **(C)** Product of volume and maximum velocity (tsunamigenic potential) and each of them alone.

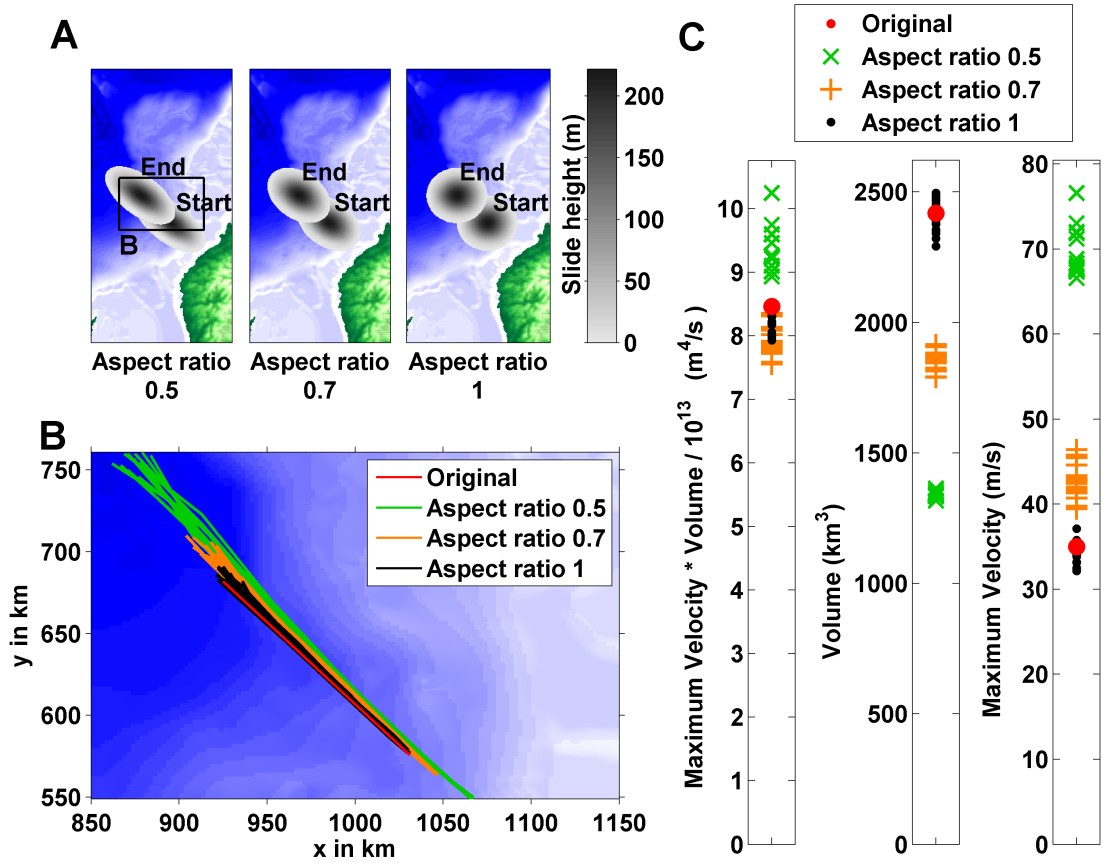

Figure 5 Influence of slide geometry on inversion results (Noise level: 20 nrad). **(A)** Slide models with identical volumes, but different aspect ratios: 0.5, 0.7 (as described in section 3.2) and 1. **(B)** Inverted and original center of mass trajectories. **(C)** Product of volume and maximum velocity (tsunamigenic potential) and each of them alone.

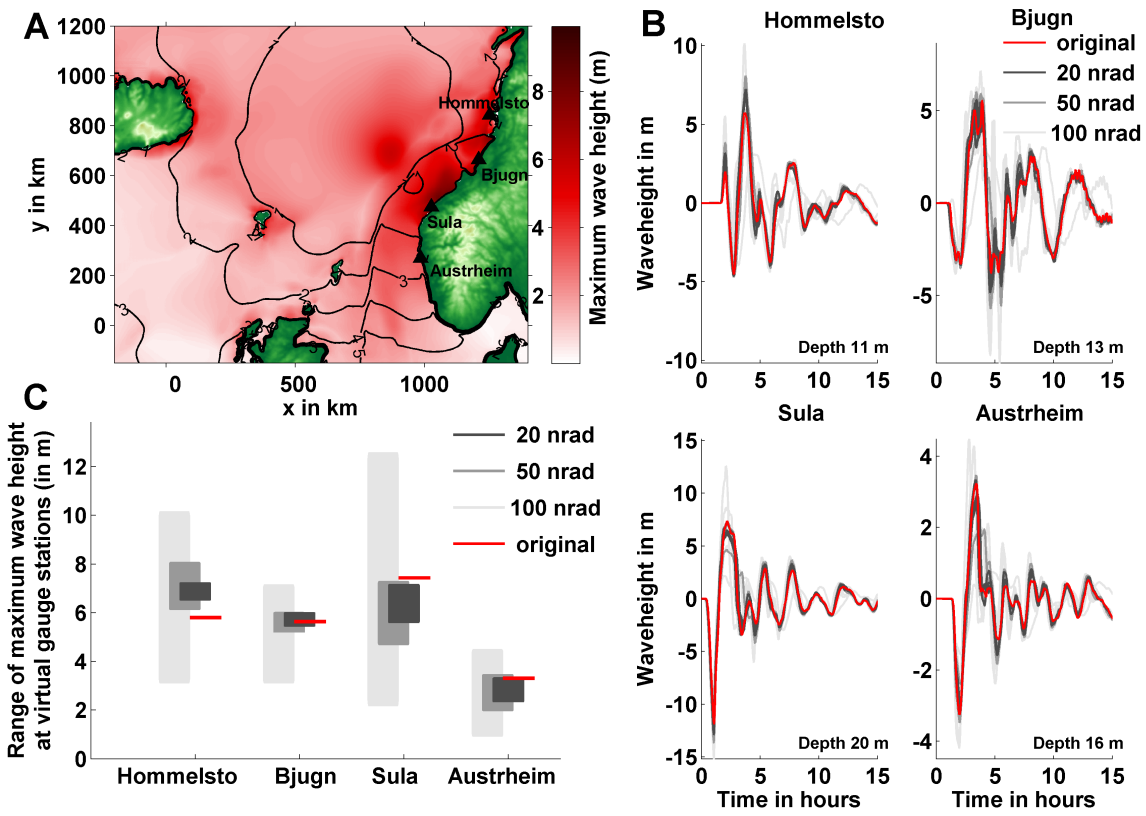

Figure 6 Tsunami prediction based on inversion results. **(A)** Maximum tsunami wave heights and arrival times of the original scenario. Positions of virtual tide gauges are marked by black triangles. **(B)** Virtual mareograms of original and inverted tsunami scenarios. **(C)** Scattering range of maximum wave heights for original and inverted data.

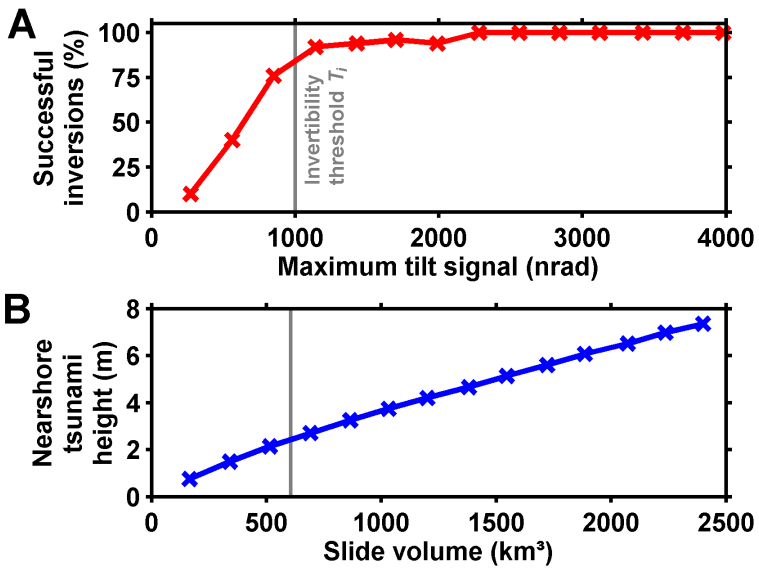

Figure 7 Defining the invertibility threshold for Storegga-like scenarios of volumes between 165 km³ and 2400 km³ (original Storegga size). **(A)** Percentage of successful inversions (inverted tsunamigenic potential within 20 % range of original one; white noise amplitude: 20 nrad) and invertibility threshold. **(B)** Invertible scenarios exceed 600 km³ and exhibit wave heights larger than 2.5 m.

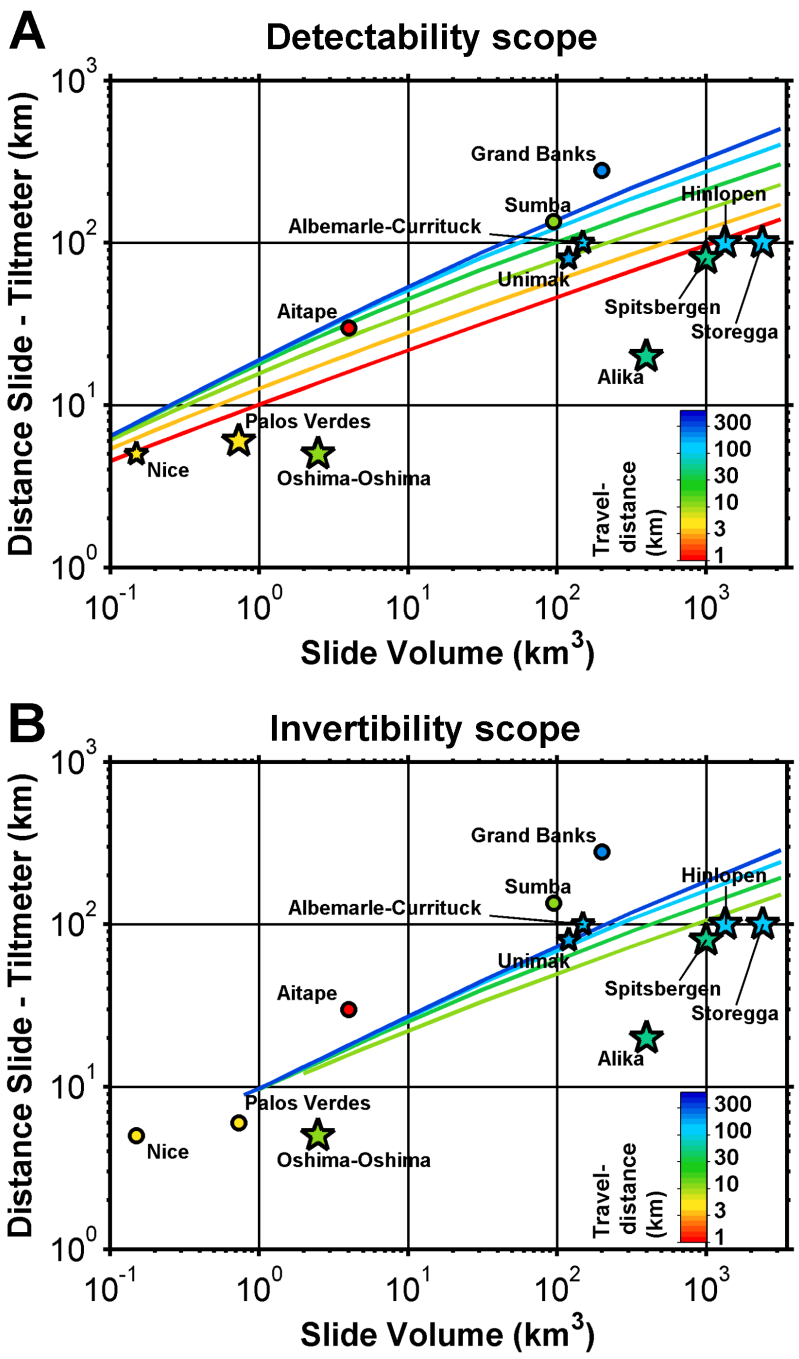

Figure 8 Applicability scope **(A)** Scope of the detection method **(B)** Scope of the inversion. Detectability and invertibility depend on three parameters: slide volume, distance between slide center-of-mass to tilt station (nearest coastal point) and travel distance of the slide center (color-coded). Stars and circles designate past or possible events (see Table 1). For data points lying below the curve of corresponding color (designated by large stars) the distance between slide and tiltmeter permits to detect/invert the event. For data points above the line (shown as circles) the distance between slide and coast is too large. Events that are located very close to the detection boundary are depicted as small stars.